Study of a down slope windstorm over Southern Norway, Rjukan, 16. January 2000

Anne Dagrun Sandvik
Knut Harstveit

Norwegian Meteorological Institute met.no

report

Title	Date
Study of a down slope windstorm over Southern Norway, Rjukan, 16. January 2000	10.12.2005

Section	Report no.
Climate	No. 18/05

Author(s)	Classification
Anne Dagrun Sandvik	☑ Free ☐ Restricted
Knut Harstveit	**ISSN** 1503-8025
	e-ISSN 1503

Client(s)	Client's reference
met.no; Norwegian Research Council	

Abstract

Strong downslope winds in the inner part of Southeastern Norway during northwesterly flow were studied. An episode with damage on the forests and power lines in the area was chosen. The situation was characterized by strong stable stratification and results from a general weather prediction model illustrate gravity waves forced by the mountain barrier. These output results were taken as input data to a nonhydrostatic mesoscale numerical model to study the resulting effects in a deep valley with steep valley sides close to the mountain plain at the lee-side of the mountains. The model reproduces very well the strong and turbulent wind that is described for parts of the valley, for instance in episodes where trains were blown off the railway. Moreover, the results indicate a twisted, S - formed wind regime induced by three-dimensional bluff body separation close to the steep valley side, and a low level jet in the valley.

Keywords
Wind, downslope, nonhydrostatic

Disiplinary signature	Responsible signature
Eirik Førland	**Cecilie Mauritzen**
_____	_____

Contents

1. Introduction

Several times, extraordinary strong winds have been reported to occur in the steep, narrow Vestfjorddalen in Telemark, Southern Norway (Figures 2 and 7). For instance, 1917 February 9, and 1926 December 12, trains were reported to have been blown off the railway. To protect the railway from further damage, an artificial soil ridge was built. On a recent occasion, 2000 January 16, parts of a forest were blown down and electrical power cables were damaged. A similar windstorm episode occurred 2001 November 15, when most of the remaining forest blew down.

All the reported episodes of extreme wind conditions in Vestfjorddalen are found in connection with west to northwest flow across southern Norway. In the situation studied, there was strong static stability connected to a cold front. An extensive review of theories explaining the origin of downslope windstorms is found in Durran (1990). According to this work the simplified physics of the two dimensional hydraulic jump may explain most downslope windstorms. Another theory explaining this phenomenon may be reflection of gravity waves from the tropopause or a critical layer.

Generally, downslope windstorms in Norway are not well documented, either from observations or from numerical studies. Our knowledge is mainly based on reports of extraordinary strong and damaging winds. Strong downslope winds in southerly fields have been studied at Oppdal (Harstveit et al. (1995), Doyle and Shapiro (2000)). In situations with strong southeasterly winds, damaging wind speeds may occur on the western side of the 1000 -2000 m high mountain ridge, for instance in the Hardanger region south of Bergen.

The Norwegian mountains, however, consist of ridges, tops and steep slopes on many scales, and the combined effects at particular localities are not well understood. At some locations, weakly stratified air masses and strong winds may cross small scale, steep, asymmetric mountains, resulting in high turbulence and corkscrews on the downstream side. Studies made at the Norwegian Meteorological Institute after the most notable windstorm in Norway in recent years, the New Year storm of 1992 (Grønås, 1995), showed that the most serious damage was found at such places (Andresen and Harstveit, 1993).

In the first part of this study, flow across southern Norway, large amplitude mountain waves and strong downslope winds connected with a cold front are briefly discussed. In the second part, we discuss the flow across the isolated valley, given the initial atmospheric conditions from the first part of the study.

2. Flow across Southern Norway

Time and again lows cross the Atlantic and approach the coast of Norway, and northwesterly winds behind the cold front frequently blow over the country. Occasionally, the wind may be strong, and high static stability connected to the cold front may strengthen the wind on the lee side of the elongated mountain barrier.
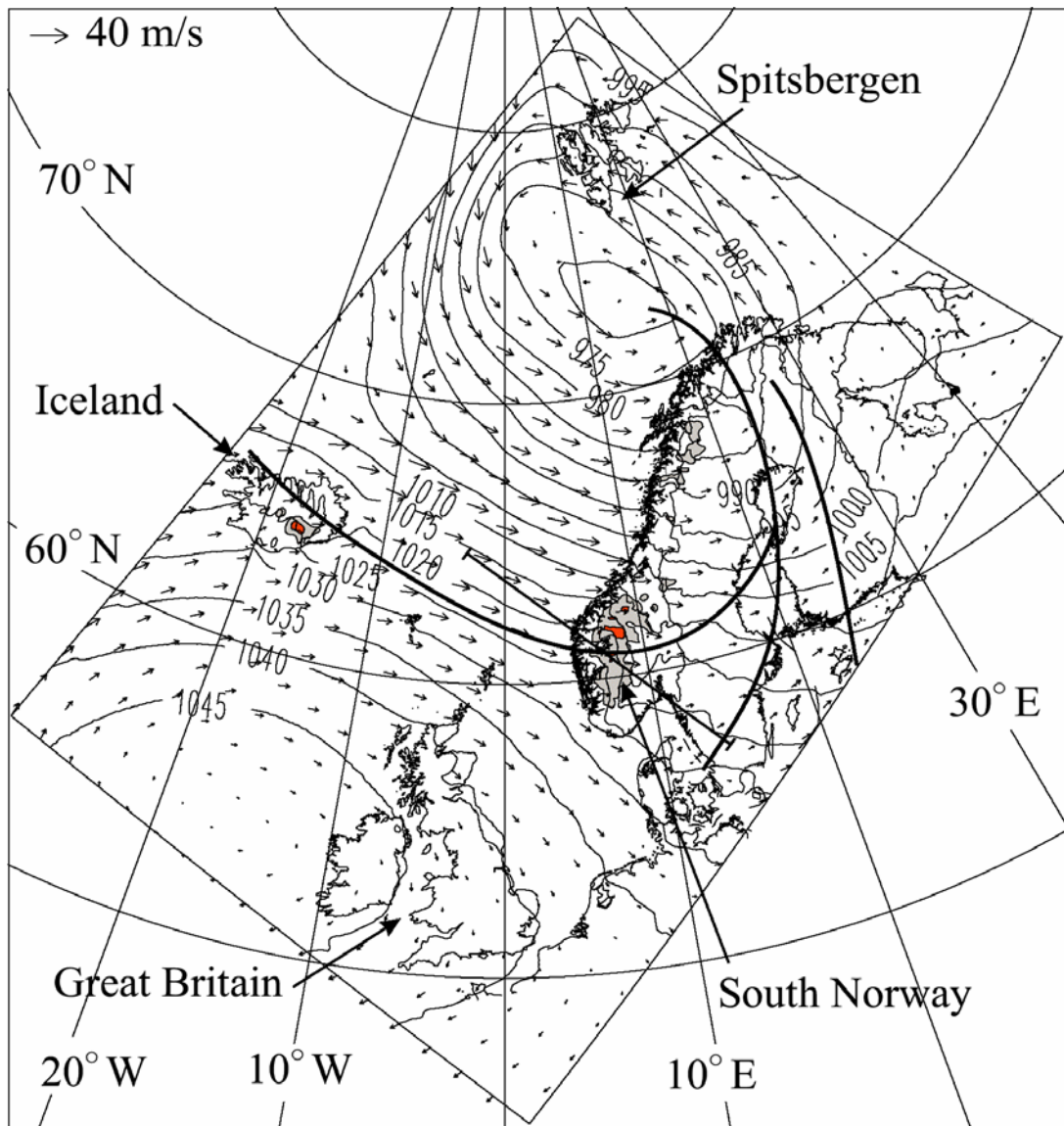
2.1 Analysing the weather situation

Figure 1

HIRLAM10 integration domain and names used in the text. The 12h prediction of sea level pressure (solid lines, 5hPa between isolines) and wind arrows valid at 1200 UTC 16 January 2000. The shaded areas show topography higher then 1000 and 1500m. Fronts are subjectively drawn. The position of the cross - section shown in Figure 3 is marked.

At the time of the damage, a high-pressure area (1045 hPa) east of Great Britain and a low-pressure area (970 hPa) between Northern Norway and Spitsbergen were found on the synoptic weather charts. The resulting northwesterly flow, about 20 m s^{-1} at the surface (Figures 1 and 2) and high static stability in the lower troposphere in connexion with a cold front, gave large amplitude mountain waves and downslope windstorms downstream of the major mountains in Southern Norway. The strong lee-side winds were well predicted by the weather prediction model at the Norwegian Meteorological Institute (NMI), HIRLAM (Gustafsson, 1993; Källén, 1996), with 10 km between the horizontal grid points. Wind force

and vectors valid at 2000 January 16, 1200 UTC are shown in Figure 2. As shown, high wind speeds are estimated at several places downstream of the large mountains (shaded grey). Areas with wind speeds exceeding 17.5 m s^{-1} are dark shaded.
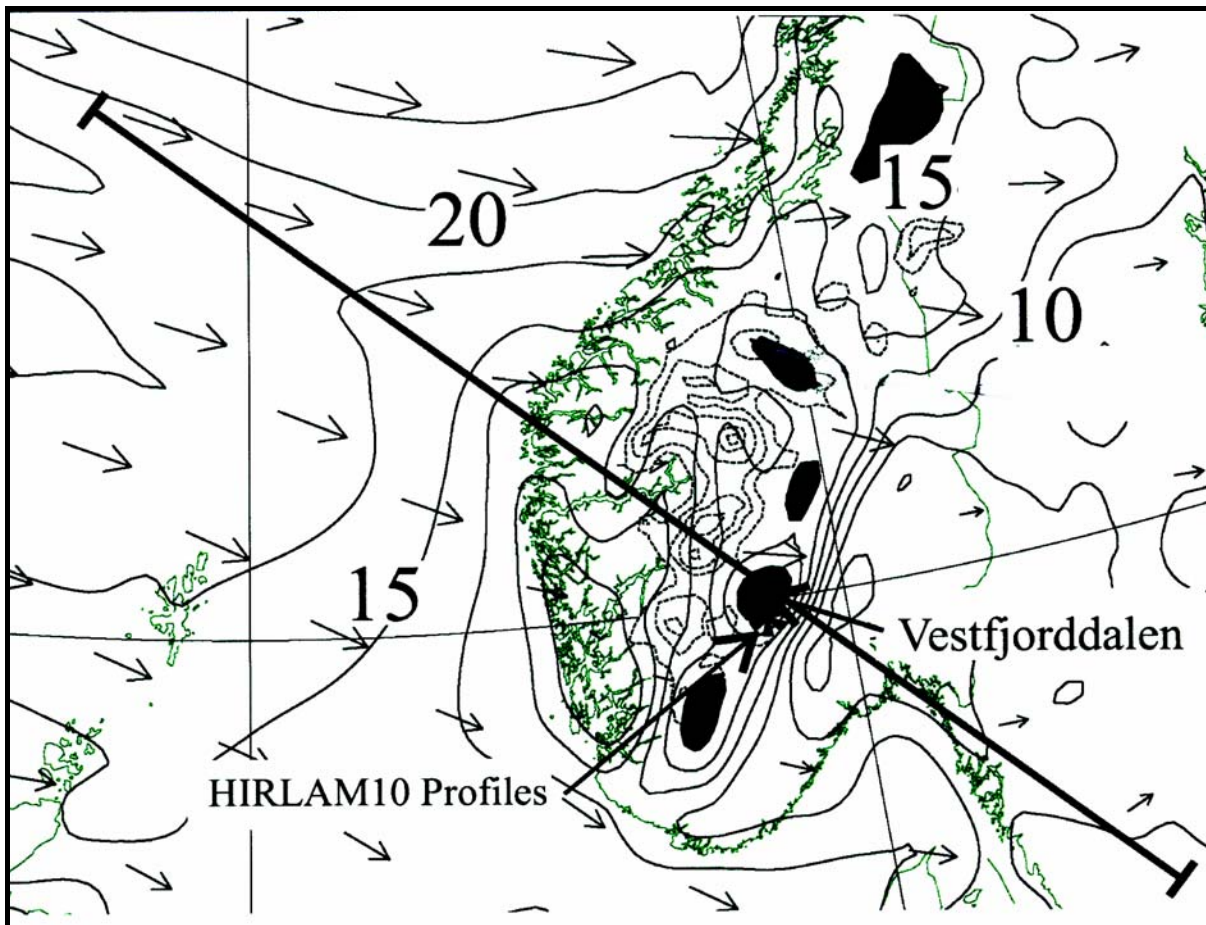

Figure 2

The 12h prediction of wind (force, solid lines, and arrows) in the lowest model level, valid 16 January 2000. Dark shaded areas shows where the downstream wind speed is stronger than 17.5 ms^{-1}. Dashed lines show topography from 1000 m asl and further lines are included to emphasize mountain tops. The position of the cross - section shown in Figure 3 is marked.

The large amplitude mountain wave is shown in Figure 3. The shaded area show a downslope wind speed higher than 40 m s^{-1}. The ow pattern was con rmed by results from a similar integration with the numerical model NORLAM (Grønås and Hellevik, 1982; Nordeng, 1986; Grønås et al., 1987) with 20 km between the horizontal grid points.
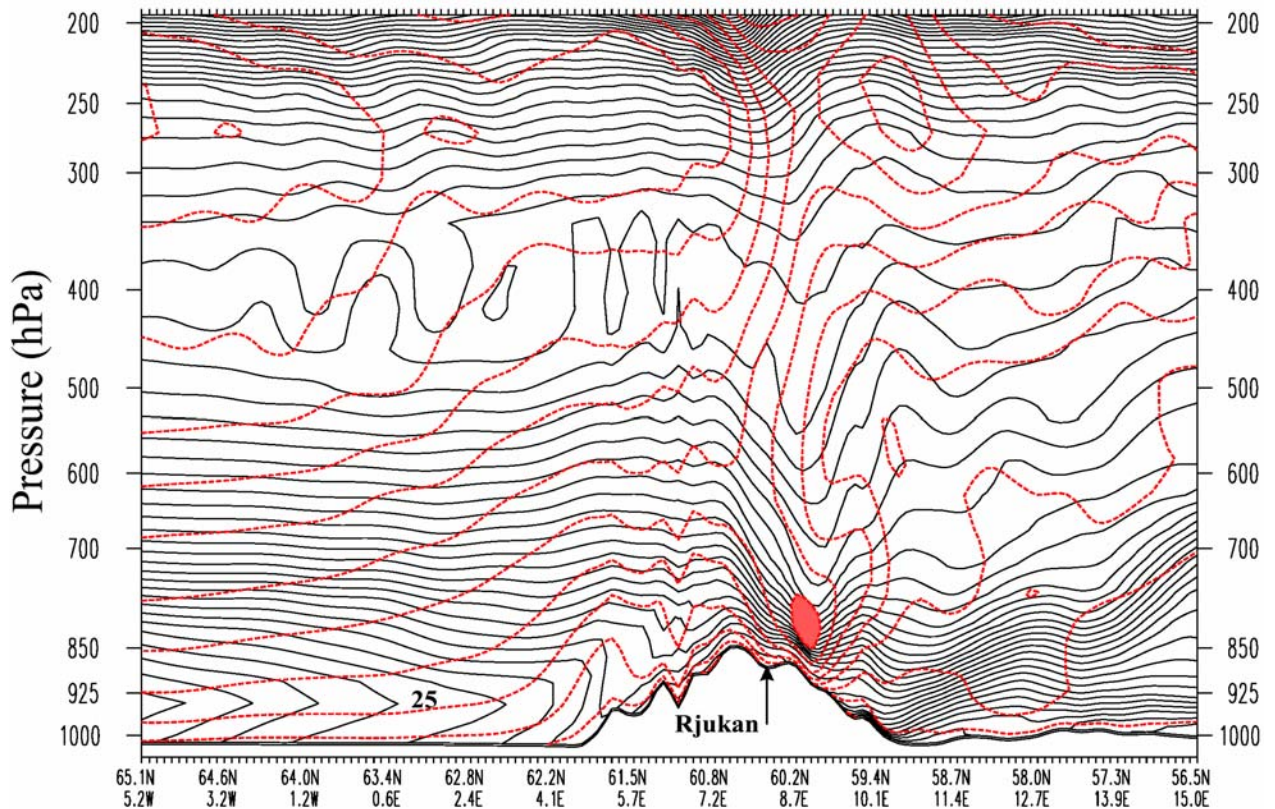
Figure 3

Cross section of the 12 h prediction of potential temperature (solid lines, 1K between lines) and horizontal velocity (dashed lines, 5 ms^{-1} between lines). The shaded area shows wind speed higher than 40 ms^{-1}.

2.2 Observations and Hirlam10 simulations

Figure 4 shows profiles of temperature, wind speed and wind direction at Ørland, Sola and Gardermoen. As seen, the observations fit the HIRLAM10 model analysis very well. Also presented (Figure 5) is an upstream temperature profile found by interpolating profiles from Sola and Ørland. We see clearly the downstream warming at Gardermoen, but at the lowest levels, a cold layer dominates (16.01.06Z). Figure 5 also shows potential temperature every hour at the west coast (Bergen), and at the area around Vestfjorddalen (Gvarv, Dalen and Våmar in the Skien-Telemark river basin). The potential temperature is seen to be substantially higher downstream the crest level (Våmar) than upstream (Bergen). During the first part of January 16, there was a typical inversion with warm air aloft (see the temperature at Våmar, 690 masl compared to the valley stations, Dalen and Gvarv (<100 masl). At the bottoms of the valleys, the rising in temperature came rather abruptly, but at different times probably due to difference in exposure of the valleys. However, the time when the cold stable air is swept out of the valleys are in relatively good accordance with a substantial (10 -15 m s^{-1}) increase in the wind speed found from the Hirlam10 simulation between 00 and 12 UTC, January 16. It is also seen that the potential temperature at the three stations in the area is the same after January 17, 00 UTC, the air masses then seem to be well – mixed.
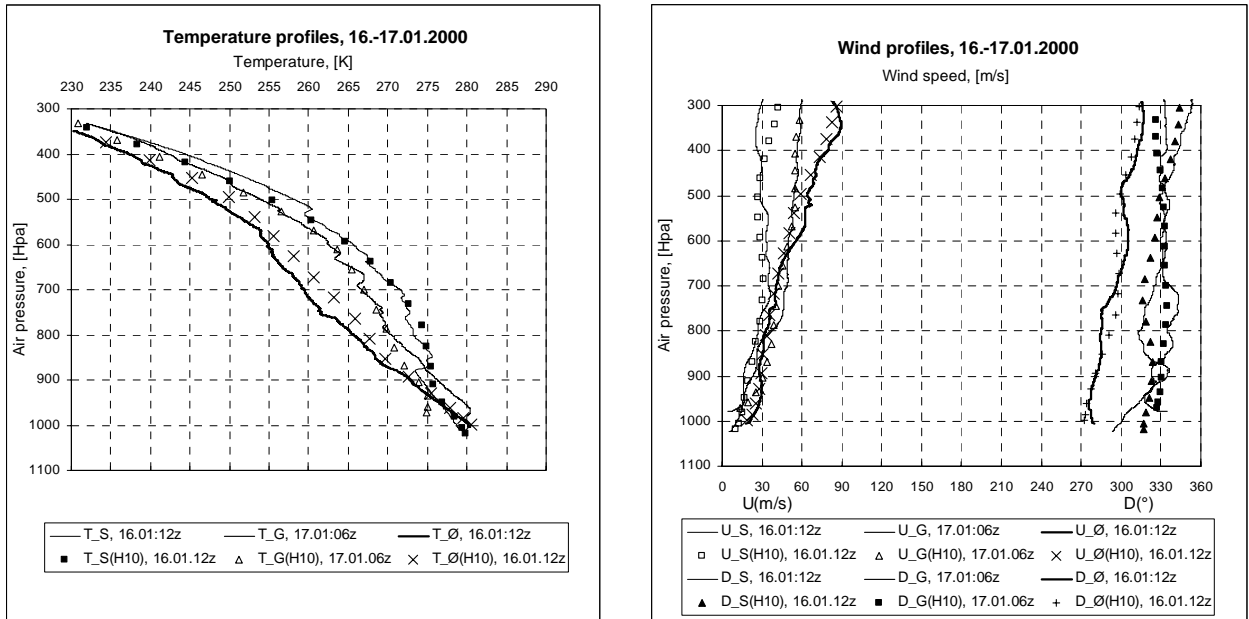
Figure 4

Profiles of temperature, T, wind speed, U, and wind direction, D, from observations and Hirlam10 analysis at the sites Sola, S, Ørlandet, Ø, and Gardermoen, G.
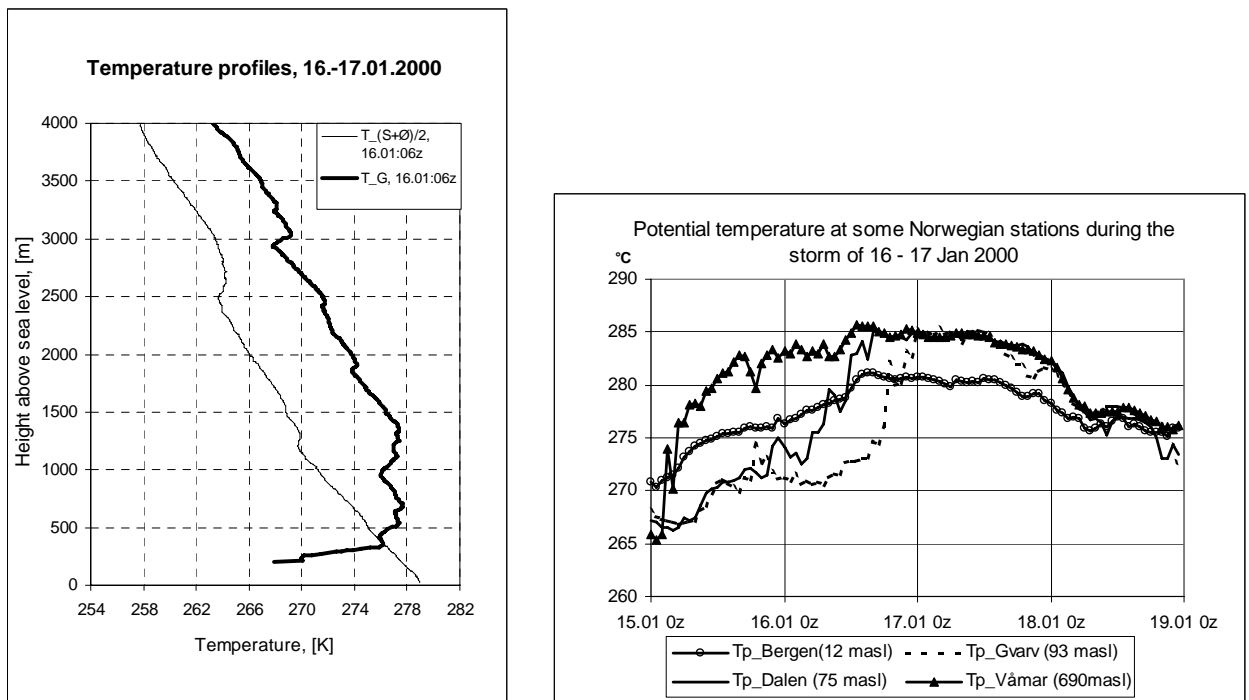

Figure 5

Potential temperature observed at some stations during the storm of 16 – 17 Jan 2000.

For use in the high resolution model integration, a vertical profile was taken from the HIRLAM10 integration (position shown in Figure 2). This profile shows a low-level jet with a maximum wind speed of 41 m s^{-1} at 900 m above the surface at a direction of 306˚ (Figure

6). At 30 m, which is the lowest level in HIRLAM10, the wind speed is 22 m s^{-1} and the direction is 298˚. The atmosphere is statically stable with an inversion in the layer from 140 to 900 m above the surface.

The Brunt-Väisälä frequency, N, is estimated to be 0.024 s^{-1} between 140 and 900 m above the surface and 0.013 s^{-1} between 900 and 3000 m.

The wind speed measured at the above stations all show gusts of up to 20 – 25 m s^{-1} throughout the period. Unfortunately, we have no wind records from the severe wind area in Vestfjorddalen where the wind gusts most probably were higher.

There was considerable forest damage in some parts of inner Telemark (e.g. Vestfjorddalen) and Aust – Agder including parts of Setesdalen. With respect to most wind directions, this is a rather sheltered area. From the damage picture, the storm can be characterized as severe, though not extremely severe.

3. The mesoscale numerical model

The nonhydrostatic mesoscale numerical model MEMO has been developed at the University of Karlsruhe and has been installed at several research institutions in Europe. Detailed descriptions of the model can be found in Flassak and Moussiopoulos (1987), Moussiopoulos (1989), Flassak (1990), Moussiopoulos (1994), and Kunz and Moussiopoulos (1995). The parameterization of clouds and precipitation has been made by Sandvik (1996, 1998). The dry version of the model has the following dependent variables: the three wind components, pressure, potential temperature, and optionally, turbulent kinetic energy (TKE) or TKE and dissipation rate ε. The vertical coordinate is a normalized height (σ_z) above the height of the mountains: $\sigma_z = H(z-h(x,y))/(H-h(x,y))$. Here z is the height above sea level and H the constant height of the top boundary.

Finite differences are used to solve the equation system on a staggered Arakawa C grid. Temporal discretization of the prognostic equations is based on the explicit second-order Adams-Bashforth scheme (Flassak, 1990). There are two deviations from this: The nonhydrostatic part of the pressure perturbation is treated implicitly, and for the vertical turbulent diffusion the second-order Crank-Nicolson method is used.

The advection scheme fulfils the following five requirements (Flassak, 1990): transportivity, positivity, conservativity, numerical stability and low numerical diffusion. The well-known upstream scheme is frequently used in mesoscale models because of its simplicity. It fulfils the four first requirements, but has the great disadvantage of strong numerical diffusion. To avoid this problem, a second-order so-called total -variation - diminishing (TVD) scheme has been developed, based upon the one-dimensional (1-D) scheme proposed by Harten (1984, 1986). This scheme combines the upstream scheme with the second-order Adams-Bashforth scheme, and has little numerical diffusion. The well-behaved advection scheme ensures reasonable results even for the shorter wavelengths. This is important for our kind of integrations, where the resolution is sometimes marginal.

The handling of the boundary conditions is always vital in our kind of limited-area modelling, and much effort has been put into MEMO on this aspect. The original radiation conditions (Orlanski, 1976) merely allow disturbances to propagate out through the boundaries, but do not allow information from outside to be imposed at the boundary. Therefore expanded radiative conditions are used at the lateral boundaries (Carpenter, 1982). For the nonhydrostatic part of the mesoscale pressure perturbation, homogeneous Neumann boundary conditions are used at lateral boundaries.

At the upper boundary, Neumann boundary conditions are imposed for the horizontal velocity components and the potential temperature. To ensure nonreflectivity, a radiative condition (Klemp and Durran, 1983) is used for the hydrostatic part of the mesoscale pressure perturbation at that boundary. Therefore vertically propagating internal gravity waves are allowed to leave the computational domain. For the nonhydrostatic part of the mesoscale pressure perturbation, homogeneous staggered Dirichlet conditions are imposed (Flassak, 1990). The lower boundary coincides with a height above ground corresponding to its aerodynamic roughness. For the nonhydrostatic part of the pressure perturbation, inhomogeneous Neumann conditions are imposed. A discussion about Neumann and Dirichlet problems may be found in, for example, the work by Copson (1975). All other conditions at the lower boundary follow from the assumption that the Monin-Obukov similarity theory is valid. Except for water surfaces, where the temperature is constant throughout the simulation, the surface temperature is calculated by solving the balance equation for the surface heat fluxes with a Newton iteration technique.

Together with the boundary conditions, the parameterization of the turbulence scheme has particular importance for our simulations. For the turbulent diffusion terms the closure assumption from the gradient transport theory is used (Stull, 1988). The value of the eddy viscosity coefficient, K_m, which is assumed to be equal in the horizontal and the vertical direction, may be computed by either a 1. or a 1.5 order closure scheme. For the 1.5 order approximation, either a one ($K_m=K_m(TKE)$) or two equation ($K_m=K_m(TKE,\varepsilon)$) turbulence scheme is used. The TKE and the dissipation rate ε are computed by prognostic equations (Flassak, 1990). The eddy diffusivity for the scalars is then calculated as a relation between the eddy viscosity and the turbulent Prandtl number.

4. Setup of the experiments

Topographical data have been taken from a square grid where the size of the grid boxes was 100 m x 100 m and interpolated to a 300 m model grid using a nine point stencil. The domain, which covers 28.8 km x 28.8 km is shown in Figure 7. The present work will be focused on the area around Vestfjorddalen. All grid points have been assumed to be land with sparse vegetation ($z_0 = 0.3$m).Vertically, the atmosphere has been divided into 25 layers, which follow the terrain. The lowest level for the main prognostic variables has been set at 10 m above the ground, and the top level has been set to 3000 m. The following levels have been used for the dependent variables: 10, 31, 55,82, 113, 147, 186, 230, 279, 335, 397, 468, 548, 638, 739, 854, 983, 1128, 1292, 1477, 1685,1920, 2185, 2484, and 2821 m above ground.
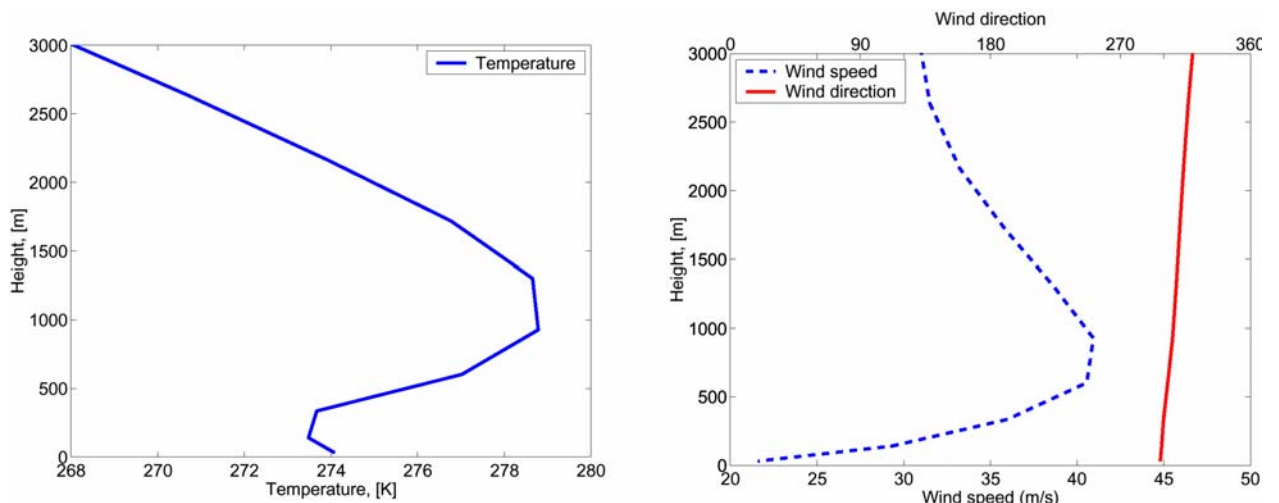
Figure 6

Profiles of temperature (K) (left), wind speed (ms⁻¹) and wind direction (degrees) (right) from HIRLAM10 valid at 1200 UTC January 16, 2000. The profiles are taken from the position marked with a star in Figure 2.

The 1.5 order closure scheme with TKE as prognostic variable has been applied. The numerical integration has been performed for one hour with a time step of 1 s and a horizontal grid increment of 300 m. A vertical profile for wind and temperature (Figure 6) has been taken from the successful HIRLAM10 prediction (the position for the profiles is on the mountain plateau, shown in Figure 2, upstream of the MEMO integration area). Lateral boundary values for this 10 km run have been provided by a HIRLAM integration with 50 km horizontal grid length on a larger domain (HIRLAM50). In this run, a numerical meteorological analysis from the Norwegian Meteorological Institute has been used as lateral boundary conditions. In the HIRLAM integrations, 31 vertical layers have been used to represent the troposphere and the stratosphere. Amass-consistent interpolation procedure (Kunz, 1991) has been used to give initial values from theHIRLAM10 profiles to all model grid points. After a spin-up time of about 20 min. the flow became approximately steady. Results after one hour of integration are presented.

5. Results from the MEMO integration

Vestfjorddalen (Figure 7) is a 14 km long, flat valley with steep slopes on both sides. It has its origin west of Rjukan, goes 7 km east, turns left, goes 7 km NE and turns right before it ends at the lake Tinnsjø. The plateau NW of the valley is about 1000-1200 masl and the plateau to the SE 800-1000 m, while the valley bottom is at about 200 m. This gives a maximum internal mountain height of about 800m. The width of the downslope side of the valley is estimated to about 2000 m and the valley width is 3500-4000 m, Figure 9d. The latter distance is represented by 13 grid lengths, which should be sufficient to resolve the cross-valley circulations. In the middle of the valley there are 16 vertical layers between the valley floor and the surrounding mountains.
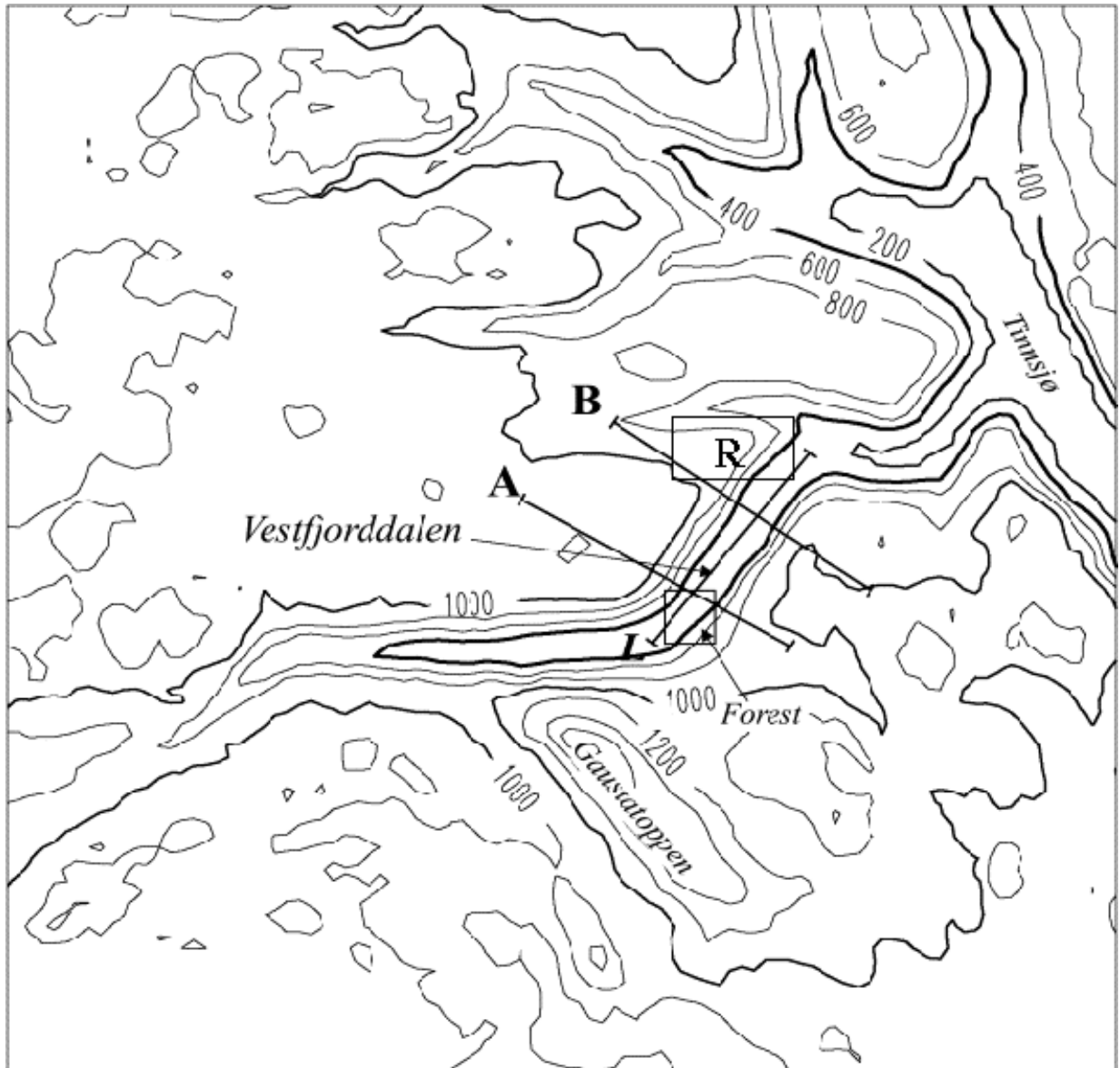
14

Figure 7

The integration domain and the topography used in MEMO (contours every 200 m). The positions of cross - sections shown in later figures are marked.

For the case of an infinite depth fluid, the displacement field over a valley is an inverted and reversed form of that over a mountain with the same shape, Baines (1995). For most cases (valley geometries, initially uniform wind and static stability profiles) sweeping flow occurs in the valley. Under certain conditions lee-side flow separation occurs. This is controlled by the atmospheric stability, the wind speed and the steepness of the downslope side of the valley.

5.1 Local flow in the valley

The horizontal wind field at every grid point 30 m above the surface is shown in Figure 8. The wind variation near the surface is seen to be highly influenced by the topography, with

velocities varying from zero to 28 m s^{-1}. The wind mainly flows along the valley, with small-scale variations both along and across the valley and with a component towards the downslope side. The along valley axis (line L in Figure 7) of Vestfjorddalen has an orientation SW -NE (210/220 – 30/40˚ relative to north), and the angle between the valley axis and the wind direction over the northeastern plateau is close to 90˚. The valley axis west of the line, L has a direction of 270 – 90˚, and the upper level wind forms an angle of 30˚ with this part of the valley. The maximum wind speed in the valley is found close to the position where line B crosses line L in Figure 7. Here the speed is about 20 m s^{-1}, and the wind direction is 177˚ (40˚ to the valley axis), which means that the along and across valley component of the wind is approximately equal (14 m s^{-1}), with the along valley component slightly higher than the cross component. Figure 9 shows the normal wind velocity, tangential wind velocity, vertical velocity, potential temperature, turbulent kinetic energy and horizontal wind speed in a section across the valley (line B in Figure 7). The down valley wind has a maximum of 18 m s^{-1} about 300 m above the valley floor, and is about 16 m s^{-1} at the floor. In the cross valley wind a recirculation area is seen below 500 m above ground. The cross valley wind is about 10 m s^{-1} toward the downslope side at the valley floor. The maximum vertical velocity is 4 m s^{-1} upward on the NW side of the valley and 7m s^{-1} downward on the SE side (Figure 9e). The circulation within the valley then has a mean across valley circulation up the NW valley side and downward on the opposite side in combination with a strong down valley wind at the bottom. The disturbed rotating flow fills the valley, and is organized like a corkscrew down the valley. From Figure 10 (similar to Figure 9, but for cross section A in Figure 7) it is seen that at this location there is a very shallow recirculation on the NW side of the valley. Comparing Figure 9 and Figure 10, we can conclude that the rotation increases down the valley, and the turbulence is found to be large, with a distinct maximum close to the point (B,L) in Figure 7 (Figure 9e, 11e), at 800 masl. In earlier work by Grønås and Sandvik (1999) it was shown that for neutral flow and similar terrain, a corresponding corkscrew was formed.
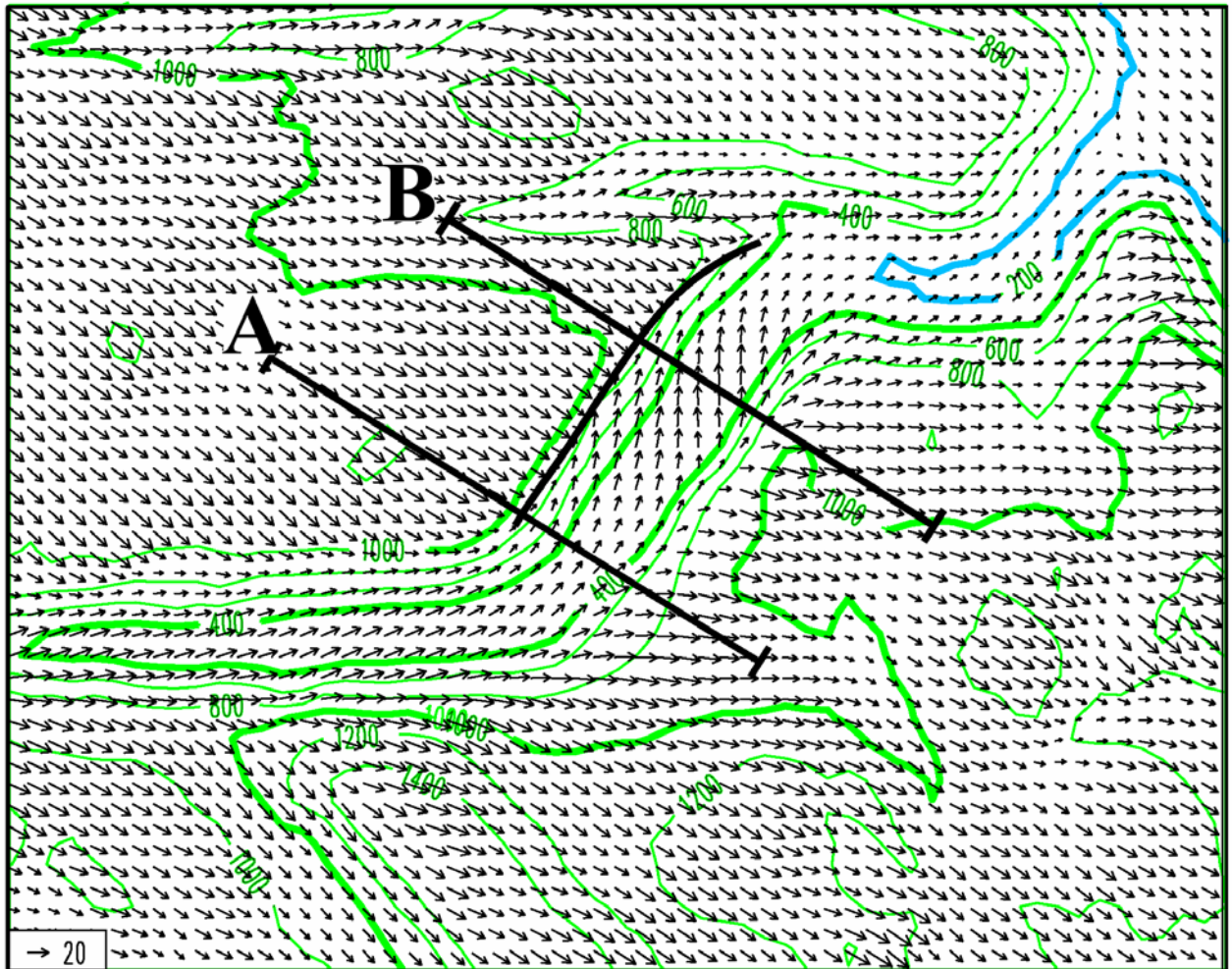
Figure 8

Predicted horizontal wind distribution, 30 m above the terrain height. Shown is also the topography. The separation line in Vestfjorddalen is shown as the solid line on the NW side of the valley.

5.2 Physical discussion

When the valley side is steep, particles flowing out over the valley do not always follow the steep terrain. Instead, the particles frequently separate from the surface and flow across the valley. This phenomenon is called lee-side bluff body separation and gives a turbulent recirculation area in the valley. For neutral stratification, separation occur if the slope angle, Arctg(h/L)>θ_c, where L and h are horizontal and vertical downslope valley dimensions measured over the maximal slope area. θc is the critical slope angle, usually not far from 20° (Finnigan, 1988), but somewhat dependent on surface roughness and geometry. According to Baines (1995), separation in a valley under stable stratification is also controlled by the nondimensional number NA_d/U, where Ad is the horizontal dimension of the down slope area, and U is the upstream wind speed. Given h/L >θ_c, separation of an idealized flow over

17

an idealized mountain/valley is found to occur for NAd/U < π, or in other words, when the horizontal dimension of the slope is less than half the wavelength of the internal waves, λ =2πU/N. In the present case NA_d/U is approximately 1.6 and Arctg(h/L)=32˚, and the condition for separation is fulfilled at several places. This can also be seen in the wind field from the model integration. The dashed (separation) line in Figure 8 indicates the position at the surface where the separation takes place. We find that when the particles flow out over the valley they follow the downslope terrain for about 100 m and separate from the underlaying air between 1000 and 800 masl, somewhat lower in the northeast.
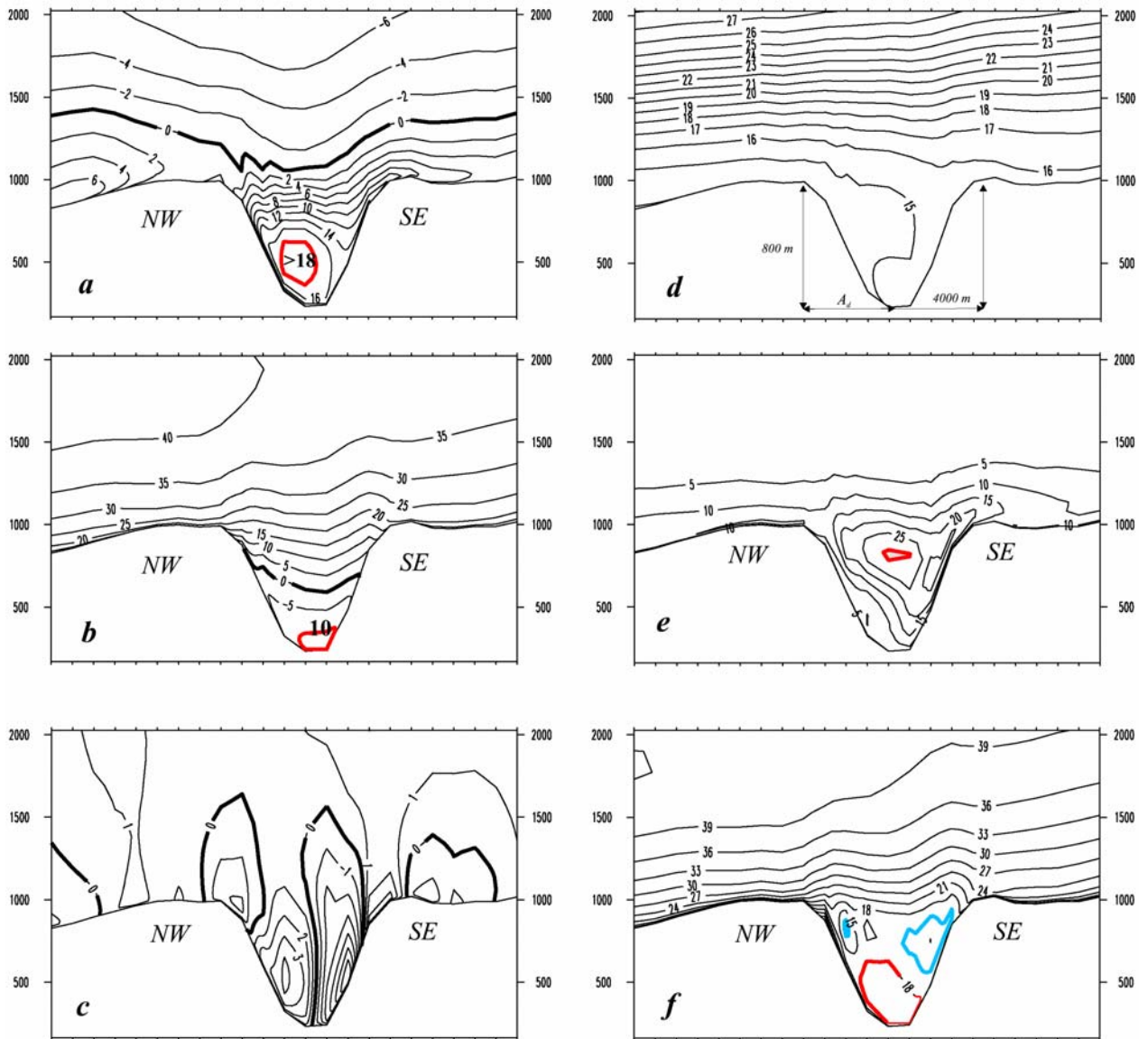

Figure 9

a) normal wind component (2 ms⁻¹ between the lines), b) tangential wind component (5 ms⁻¹ between the lines), c) vertical wind component (1 ms -1 between the lines), d) potential temperature (1 K between the lines), e) turbulent kinetic energy, TKE, (5 m² s⁻² between the lines), and f) horizontal wind velocity (3 ms⁻¹ between the lines) in cross - section B.
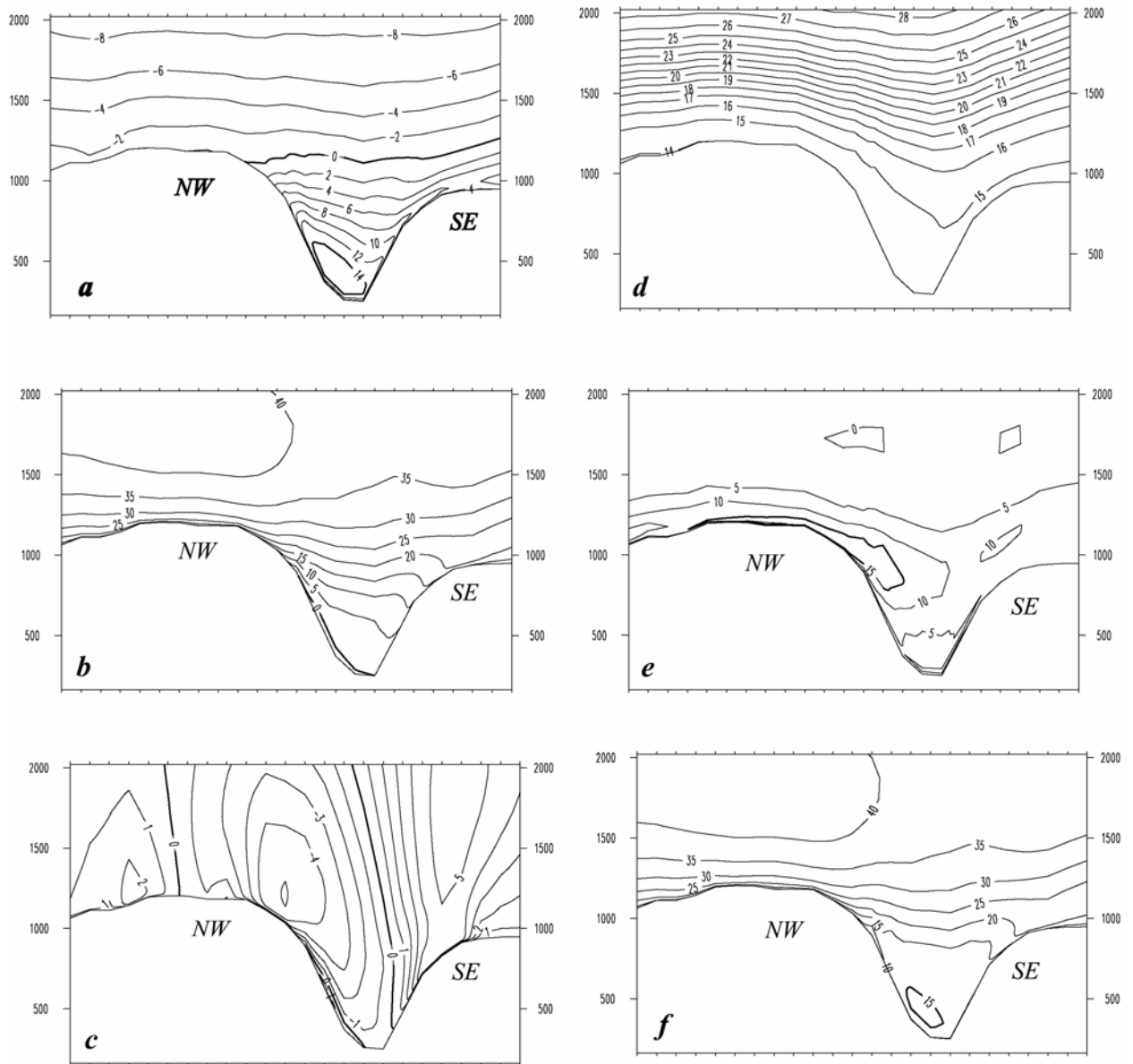
Figure 10

a) normal wind component (2 ms^{-1} between the lines), b) tangential wind component (5 ms^{-1} between the lines), c) vertical wind component (1 ms -1 between the lines), d) potential temperature (1 K between the lines), e) turbulent kinetic energy, TKE, (5 m^2 s^{-2} between the lines), and f) horizontal wind velocity (3 ms^{-1} between the lines) in cross - section A.

Figure 11 shows that the turbulence maximum is found in an area where the wind direction changes rapidly from a wind along the valley to the stronger cross wind higher up. Obviously, this is also connected to a low level yet below the region of maximum turbulence (Figures 9e-f, 11 e-f).

Wind gusts can reach values 2 -3 times the mean wind speed in turbulent areas close to steep mountains, so, gusts well above 40 m s^{-1} can be expected in the valley bottom.
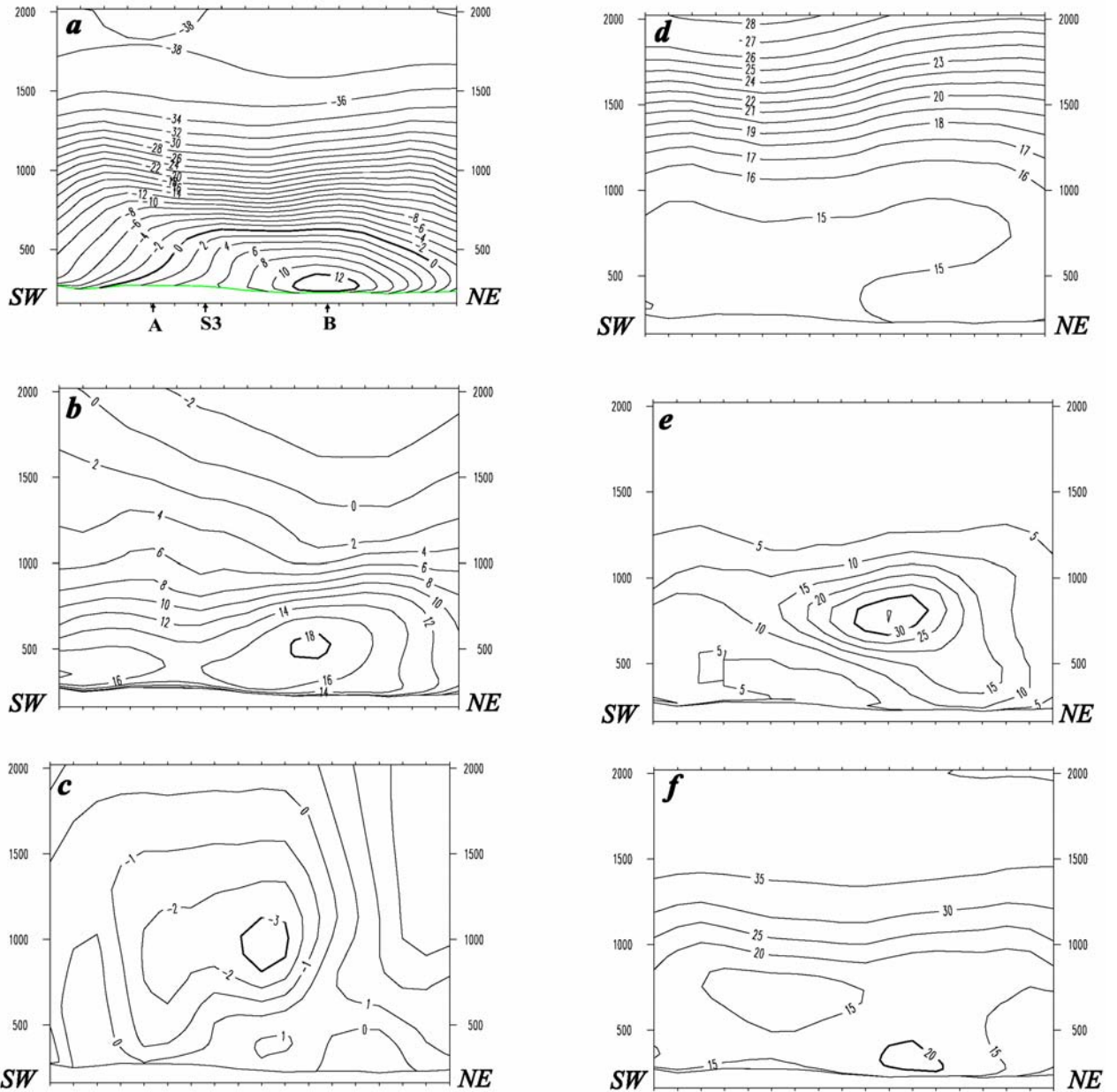
Figure 11

a) normal wind component (2 ms^{-1} between the lines), b) tangential wind component (5 ms^{-1} between the lines), c) vertical wind component (1 ms^{-1} between the lines), d) potential temperature (1 K between the lines), e) turbulent kinetic energy, TKE, (5 m^2 s^{-2} between the lines), and f) horizontal wind velocity (3 ms^{-1} between the lines) in cross - section L.

The present valley may be said to have two valley axes. The western part has a direction of 270 – 90˚, and the upper level wind forms an angle of 30˚ with the valley. There is a strong down valley component at low levels. Further east the flow comes more perpendicular to the valley and a rotor is probably formed. At the ridge, R, north of the eastern part of the valley close to section B (Figure 7), a strong wind enters the 500 – 1000 m level and blows across the valley at lower heights as we move downwards along the ridge. A vertical wind shear causes a drag on the air below and a horizontal shear causes a drag on the air to the right. The steep terrain makes the wind separate and the vertical shear makes it rotate. The

20

horizontal shear stretches the rotor. This gives us a picture of a twisted S-shaped belt, from the plateau N of Rjukan, down through the corner and the valley bottom between A and B, up along the ridge close to B and further up and along the plateau – wind. Also air stream from the plateau west of section A is rotated down the valley. This circulation follows the topography and reduces the large resistance due to the steep hill at the western valley side between A and B, and brings strong and turbulent wind to the valley bottom.

6. Summary and concluding remarks

The weather situation in Southern Norway, on January 16, 2000 was studied. The situation was characterized by northwesterly winds aloft and strong stable stratification. Results from a general weather prediction model show gravity waves forced by the mountains. Strong and damaging wind gusts and high temperatures were transported down the lee-side of the mountain barrier.

Vertical profiles of temperature and wind vectors were taken from the HIRLAM10 results. These profiles were used as input data to a nonhydrostatic mesoscale numerical model to study the resulting effects in Vestfjorddalen, a deep valley with steep valley sides close to the mountain plain on the lee side of the mountains. This valley is well known for episodes of strong wind gusts during west-northwesterly upstream wind directions.

In spite of the strong static stability, but in accordance with theoretical assumptions, a strong vertical wind shear and bluff body separation occur when the wind blows from the plateau and crosses the steep valley sides, inducing a rotor. On a ridge north of the eastern part of the valley, strong wind blows across the valley at lower heights as we move downwards along the ridge. A vertical wind shear causes a drag on the air below and a horizontal shear causes a drag on the air to the right. The steep terrain makes the wind separate and the vertical shear makes it rotate. The horizontal shear stretches the rotor to form a powerful corkscrew. In the upper parts of the valley, the valley axis turns westerly and the valley side are directed at a 30˚ angle to the plateau wind. The wind is then easily transported down to the valley floor, feeding the stretched rotor.

This gives us a picture of a twisted S-shaped belt, from the plateau, down through the corner and along the valley bottom, and further up the lee slope. This circulation follows the topography and reduces the large resistance due to the steep hill at the western side valley, and brings strong and turbulent wind to the valley bottom.

The model reproduced the wind regime which is described for the valley very well, for instance during episodes where trains were blown off the railway. The results from the numerical integrations gave new knowledge about the reason for the strong wind gusts and the vertical structure during the special wind conditions that may occur in Vestfjorddalen. Also, it proved that bluff body separation close to steep terrain occurs during period of strong stability and mountain waves in Norway. It will be interesting to transfer this knowledge to similar investigations at other locations.

7. Acknowledgments

8. References

Andresen, L. and Harstveit, K., 1993: Extreme value analysis for Møre og Romsdal. DNMI/ KLIMA 07/93, pp. 1-27. Norwegian Met. Inst., Oslo, Norway. (In Norwegian).

Baines, P.G., 1995: *Topographic Effects in Stratified Flows*, Cambridge Monogr. Mech., Cam-bridge Univ. Press, New York, 482 pp.

Carpenter, K.M., 1982: Note on the paper "Radiation condition for the lateral boundaries of limi-tied area numerical models" by Miller, M.J. and A.J. Thorpe, 1982, Q.J., 107, 615-628, *Q.J.R. Meteorol. Soc.,* 108, 717-719.

Copson, E.T., 1975: *Partial Differential Equations,* Cambridge Univ. Press, New York. 280 pp.

Doyle, J.D., and M.A. Shapiro, 2000: A multi-scale simulation of an extreme down slope wind-storm over complex topography. *Meteorology and Atmospheric Physics*, Vol. 74, Issue 1-4, pp 83-101.

Durran, D. R., 1990: *Mountain Waves and Downslope Winds*, Atmospheric Processes over Com-plex Terrain, W. Blumen, Ed., American Met. Soc. Vol. 23, No. 45, 59 - 82.

Finnigan, J.J., 1988: Air flow over complex terrain. *Flow and transport in the natural environ-ment: Advances and applications* (eds.: Steffen, W.L. and Denmead, O.T.), Springer-Verlag.

Flassak, T., 1990: Ein nicht-hydrostatisches mesoskaliges Modell zur Beschreibung der Dynamik der planetaren Grenzschicht., *Fortschr. -Ber. VDI Reihe 15*, VDI - Verlag, Düsseldorf.

Grønås S. and O. E. Hellevik, 1982: A limited area prediction model at the Norwegian Meteoro-logical Institute. *Techn. Rep.* no. 61. Norwegian Meteorological Institute, Oslo, Norway.

Grønås S., A. Foss, and M. Lystad, 1987: Numerical simulations of polar lows in the Norwegian Sea. *Tellus* 39 A, 334-353.

Grønås S., 1995; The seclusion intensification of the New Year's day storm 1992., Tellus 47A.

Grønås, S. and A.D. Sandvik, 1999: Numerical simulations of local winds over steep orography in the storm over north Norway on October 12, 1996. *Journal of Geophysical Research*, Vol. 104, NO.D8, 9107-9120.

Gustafsson, N., 1993: HIRLAM 2 final report, *HIRLAM Tech. Rep.*, 9, 126 pp., Swed. Meteorol. and Hydrol. Inst., Norrköping, Sweden.

Källén, E., 1996: *HIRLAM documentation manual, system 2.5*, Swed. Meteorol. and Hydrol. Inst., Norrköping., Sweden.

Harstveit, K., L. Andresen, and K.H. Midtbø, 1995: Downslope windstorms at Oppdal,

Norway. Local description and numerical simulations. *DNMI/KLIMA* 23/95, pp. 1-13 (part I), 1-29 (part II). Norwegian Met. Inst., Oslo, Norway.

Harten, A., 1984: On a class of high resolution total-variation-stable finite-difference schemes, *SIAM J. Numer. Anal.,* 21, 1-23.

Harten, A., 1986: On a large time-step high resolution scheme, *Math. Comput.,* 46, 379-399.

Klemp J.B., and D.R. Durran, 1983: An upper boundary condition permitting internal gravity wave radiation in numerical mesoscale models, *Mon. Weather Rev.,* 111, 430-444.

Kunz, R., 1991: *Enwichlung einen diagnostischen Windmodells zur Berechnung des Anfangzu-standes für das dynamiche Grenzschichmodell MEMO*, Diplomarbeit, Univ. Karlsruhe, Karls-ruhe, Germany.

Kunz, R., and N. Moussiopoulos, 1995: Simulation of the wind field in Athens using refined boundary conditions. *Atmos. Environ.,* 29, 3575-3591.

Moussiopoulos, N., 1989: *Mathematische Modellierung mesoskaliger Ausbreitung in der Atmos-phäre*. VDI-Verlag, Düsseldorf, Germany. 307 pp.

Moussiopoulos N., 1994*: The EUMAC Zooming Model, Model structure and application*, EURO-TRAC International Scientific Secretariat, Garmisch-Partenkirchen, Germany.

Nordeng, T.E., 1986: Parameterization of Physical processes in a Three-Dimensional Numerical Weather Prediction Model. *Technical Report* no.65, Norwegian Met. Inst., Oslo, Norway.

Orlanski, J., 1976: A simple boundary condition for unbounded hyperbolic flows, *J. Comput. Phys.,* 21, 251-269.

Sandvik, A. D., 1996: *Condensation processes in a non - hydrostatic mesoscale model*. PhD. The-sis, Geophysical Institute, University of Bergen, Norway.

Sandvik, A. D., 1998: Implementation and validation of a condensation mesoscale scheme in a nonhydrostatic mesoscale model, *Mon. Weather. Rev.,* 126, 1882-1905.

Stull, R. B., 1988: *An Introduction to Boundary Layer Meteorology*. Kluwer Academic Publishers, 666 pp.